Turkish Journal of Electrical Engineering & Computer Sciences

http://journals.tubitak.gov.tr/elektrik/

Research Article

Turk J Elec Eng & Comp Sci
(2023) 31: 312 – 322

doi:10.55730/1300-0632.3986

Design and modeling of a PVDF-TrFe flexible wind energy harvester

Berkay KULLUKÇU, Levent BEKER*
Mechanical Engineering, Graduate School of Science and Engineering, Koç University, İstanbul, Türkiye

Received: 05.09.2022 • **Accepted/Published Online:** 07.01.2023 • **Final Version:** 23.03.2023

Abstract: This study presents the simulation, experimentation, and design considerations of a Poly(vinylidene fluoride co-trifluoroethylene)/ Polyethylene Terephthalate (PVDF-TrFe / PET), laser-cut, flexible piezoelectric energy harvester. It is possible to obtain energy from the environment around autonomous sensor systems, which can then be used to power various equipment. This article investigates the actuation means of ambient vibration, which is a good candidate for using piezoelectric energy harvester (PEH) devices. The output voltage characteristics were analyzed in a wind test apparatus. Finite element modeling (FEM) was done for von Mises stress and modal analysis. Resonance frequency sweeps, quality factors, and damping ratios of the circular plate were given numerically. For a PVDF-TrFe piezoelectric layer thickness of 18 µm and 1.5 mm radius, a damping ratio of 0.117 and a quality factor of 4.284 was calculated. V_{max} was calculated as 984 mV from the wind setup experiments and compared with the FEM outputs.

Key words: PVDF-TrFe, piezoelectricity, wind energy harvesting, finite element modeling, vibration, frequency response

1. Introduction

Microelectronics' inclusion and rapid development have profoundly impacted human society in recent decades. The widespread availability of intelligent electronic devices paved a way for a surge of varied applications that may improve one's quality of life in a variety of different ways. Concurrent advancements in microelectromechanical systems (MEMS) technologies have resulted in improved device performance with reductions in size, cost, and the amount of power they use. Observing temperature, light, and the position of individuals in commercial properties to regulate the environment in a manner that is more energy-efficient, detecting dangerous chemical agents in high-density areas, monitoring the formation of fatigue cracks on aircraft, monitoring the speed and pressure in vehicle tires, and a great deal more are all examples of the many applications of this technology. Numerous experts believe that very low-power embedded electronic devices will become ubiquitous, performing tasks ranging from factory automation to entertainment. However, the performance of such new advancements is reliant on the availability of reliable sources of energy in the near future. As batteries and other types of energy sources that have a set capacity present a number of challenges due to their cost, size, and longevity, the device presented in the article, is intended to provide the necessary power for electronic devices by harvesting vibrational energy. Table (1) shows the comparison of macro and micro-scale energy harvesters from the literature.

In the present paper, the proposed device is intended to cater to the requirements imposed by energy harvesters. Because of its simplistic design, it is easy to implement using conventional methods, which enables the production of sensors of a comparatively compact size. The equipment in question needs to be examined to

*Correspondence: lbeker@ku.edu.tr

provide evidence supporting these statements. As a result, this study aims to accomplish two things: first, it will present and compare different techniques of analysis of the proposed device, and second, it will determine whether or not the suggested device is a viable choice for energy harvesting showing a reasonable voltage output extracted from a wind test setup in addition to the simulated performance results.

The rest of the paper is organized as follows. Section 2 presents the current literature in PVDF-TrFE, shows the proposed energy harvester design and analytical & FEM modeling. In Section 3, the proposed testing setup is presented with the experimental outputs and conclusions will be drawn in Section 4.

Table 1. Energy harvester parameters compared.

Paper	Dimensions	Shape	Voltage Output	Power Output	Resonance Frequency
[1] Qian, F. et al.	150x19x3 mm for single beam	Venus flytrap shape	Reported in figures	0.193 mW	78.35 rad/s
[2] Li, X. et al.	110x22 mm	Sandwich structure	6.21 V max. at a resonance peak	Reported in figures	18.18 Hz, 24.74 Hz, and 28.12 Hz
[3] Ramírez, J. M. et al.	Bar 1 to 10: B1:74x14x0.5 mm B2:28x14x0.3 mm B3:85x13x0.5 mm B4:59x13x0.5 mm B5:50x15x1 mm B6:50x15x2 mm B7:28x14x1 mm B8:16x10x5 mm B9:16x10x6 mm B10:15x13x2 mm	Cantilever assembly: 4 Aluminium bars & 6 Steel bars vibrating as a single body	6 V_{max}	200 µW	4.7 Hz
[5] Morimoto et al.	18.5x5 mm cantilever	Cantilever	2.6 V	244 µW	126 Hz
[6] Horowitz et al.	Thickness: 3 µm, radius: 1.85 mm	Circular diaphragm	4.6 mV	0.34 µW/cm^2 power density	3.7 kHz
[7] Wang et al.	∼2mm^2	Nanowire	Reported in figures (mV range)	Reported in figures	∼3 MHz
[8] Hu et al.	1.5×0.5 cm	Nanowire	1.5 V	70 µW/cm^3 power density	Not given
[10] Lin et. al.	500 nm x 6 µm nanowire	Nanowire	8V	∼5.3 mW/cm^3	Not given

2. PVDF-TrFe energy harvester modeling

2.1. Material search

The polymer PVDF-TrFe is selected for this application for various purposes. First of all, it can be stretched in both the longitudinal and the transverse directions, which allows it to be used to form a bioriented film [11]. As it has been proven that poled PVDF is an excellent candidate for the fabrication of piezoelectric films, the PVDF-TrFE copolymer, which has superior properties in terms of different piezoelectric coefficients, may also be poled and used instead [11]. This particular copolymer will crystallize immediately in β form as a result of the replacement of a few of the VF2(CH2- CF2) molecules in the PVDF with VF3 (CH-CF3) molecules [11].

In the study of Mohammadi et al., Fourier transforms infrared spectroscopy was used to evaluate the influence of biaxial orientation and deformation rate on the microstructure of stretched PVDF samples, and wide-angle X-ray diffraction was used to confirm the findings of the FTIR analysis [12]. FTIR spectroscopy is a well-established method for determining whether or not there has been a shift in the amount of β-phase present in PVDF films. It has been demonstrated that an additional transition of the nonpolar α phase into the polar β crystallites occurs when the stretching rate is 10–50 cm/min [12]. Polarized PVDF films have fairly balanced piezoelectric activity in the flm plane, unlike uniaxially oriented PVDF films, which have more significant piezoelectric coefficients [13]. This is because polarized PVDF films are oriented in two orthogonal directions. The crystalline structure of PVDF is directly responsible for the material's electrical characteristics [14–18].

Today, various different polar crystals have been described for PVDF. These modifications are designated as β (form I), γ (form III), δ (form IV), and ε (form V) [19]. Only when the stretch ratio is more than five is the melt-crystallized PVDF capable of being transformed into the β-phase [20]. In order to produce polar β-phase PVDF straightforwardly, one must either cast PVDF from solutions of hexamethyl phosphoric triamide or quench molten PVDF under high pressure. Both of these processes are required. Both of these methods produce the same result [20]. The electrical charge in the matching PVDF film is significantly lower than that in the 55 mol percent VDF copolymer, which has the biggest dielectric constant and the most considerable electric current [12]. An uncommon negative longitudinal piezoelectric effect was seen by Katsouras et al. in the ferroelectric polymer poly(vinylidene fluoride) (PVDF), as well as its copolymers with trifluoroethylene (P(VDF-TrFE)) [21]. It seems inconceivable that the polarization-biased electrostrictive contribution of the crystalline component is the only factor responsible for this event [21]. Electromechanical contact between crystalline lamellae and amorphous areas is the cause [21]. The so-called dimensional model, a commonly accepted explanation for the negative piezoelectric effect of PVDF, assumes that the dipoles are stiff and maintain their fixed moment and orientation even when the material is mechanically deformed [21].

According to Katsouras et al., applying a positive stress perpendicular to the chains mainly increases the distance between the chains. This is because the interactions between the chains, both van der Waals and electrostatic, are relatively weak. This dipole-induced piezoelectricity process has been verified using quantum mechanical simulations for single-crystalline polymers [22, 23]. P(VDF-TrFE) crystallizes into needle-shaped domains, whereas PVDF films consist of massive lamellae, which spread outward from the center. Table (2) shows the superiority of PVDF-TrFE compared with other widely used piezoelectric materials in terms of voltage output key performance indicator (KPI). PVDF-TrFE has 15.8% higher d_{33} value compared to homopolymer PVDF [24].

As given in (1) and (2), the g_{33} constant is directly proportional to the voltage output of the piezoelectric

Table 2. Piezoelectric material parameters compared.

Parameter	$BaTiO_3$ [27,29]	Quartz [31,32]	PZT4 [26,31,33]	PZT5H [25,28,31]	PVDF-TrFe [26,30]
g_{33} [10^{-3}]	13.06	51.98	25.12	19.71	456.79

material. PVDF-TrFe has one order of magnitude higher g_{33} constant than most piezoelectric materials.

$$V = g_{33} ds \tag{1}$$

$$V = g_{33} dE\varepsilon \tag{2}$$

2.2. Proposed design

The device operates under wind vibration. Figure (1) presents an illustration of the device's functionality and the 3D representation. Wind vibration deforms the piezoelectric plates and creates AC voltage and current. The power harvester can power up low-power electronics or charge electrical storage devices.

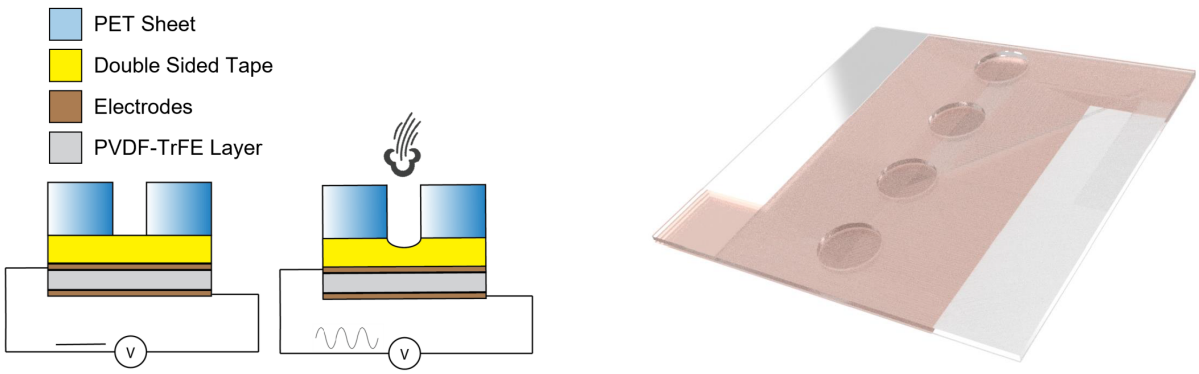

Figure 1. Working principle of the fabricated harvester: a) Circular plates vibrate under wind pressure, an Arduino-controlled fan was used for wind flow in the experiments and ambient wind will be the pressure source in a real use case b) A 3D representation of the proposed PVDF-TrFe harvester.

To fabricate the device, plain PET sheets were cut to 10 mm by 10 mm using a mechanical cutter. The sheets had a thickness of 140 µm and were laser-cut to create 3 mm in diameter circular perforations. The PET was then covered with a double-sided tape measuring 65 microns in thickness, and PolyK PVDF film was adhered to the sheet. In addition, the tape served as the harvester's structural layer, shifting the piezoelectric layers away from the neutral axis.

2.3. Energy harvester modeling

To model the energy harvester, an electromechanical equivalent circuit was used. In the circuit, there is a capacitor in the electrical domain and spring and mass elements in the mechanical domain [34].

$$C = \varepsilon \pi {r_{pm}}^2 / t_{pvdf}. \tag{3}$$

where ε is the ratio of PVDF's relative permittivity to the permittivity of a vacuum, t_{pvdf} is the thickness of PVDF, and r_{pm} is the radius of the top electrode. With a normal plate deflection shape function of $\varphi(x)$ [35]:

$$\varphi(x) = (1 - x_\vartheta{}^2)^2 \tag{4}$$

where x_ϑ is the normalized version of the radial coordinate. The axisymmetric plate deflection is given by $w(x_\vartheta) = w_0\varphi(x)$, where w_0 is the static plate deflection at the center of the clamped plate. I_m, the piezoelectric coupling integral, and I_e, the strain energy integral, can be calculated using the formulas [34]:

$$I_m = 1/(1 - v)\int_0^\gamma ((x_\vartheta d^2\varphi(x_\vartheta)/dx_\vartheta{}^2) + (d\varphi(x_\vartheta)/dx_\vartheta))dx_\vartheta \tag{5}$$

$$I_e = \int_0^1 ((x_\vartheta d^2\varphi(x_\vartheta)/dx_\vartheta{}^2)^2 + 2v(d\varphi(x_\vartheta)/x_\vartheta dx_\vartheta)(d^2\varphi(x_\vartheta)/dx_\vartheta{}^2) + (d\varphi(x_\vartheta)/dx_\vartheta))dx_\vartheta \tag{6}$$

where v is the effective Poisson's ratio of the composite plate and M is the piezoelectric bending moment supplied by the piezoelectric material [36]:

$$M = -e_{31,f}V_{in}z \tag{7}$$

$e_{31,f}$ is the transverse piezoelectric coefficient. V_{in} is the applied voltage. In addition, z is the distance between the midplane of the active PVDF layer and the neutral plane. Notably, the piezoelectric coupling integral I_m is only calculated across the electrode region (normalized radial coordinate 0 to), whereas the strain energy integral I_e is calculated throughout the entire radius. The location of the composite plate structure's neutral plane z, is determined by the following:

$$z = \sum_{k=1}^{2}(t_k z_k E_k/1 - v_k^2)/\sum_{k=1}^{2}(t_k E_k/1 - v_k^2) \tag{8}$$

The subscripts represent the thin plate layers from the harvester's base in ascending order. E_k is Young's Modulus, Poisson's ratio equals v_k, and each layer's central axis is z_k. Similarly, the flexural rigidity, D [37], and effective mass per unit area, μ_{eff} of the composite plate are:

$$D = \sum_{k=1}^{2} 1/2((h_k - z)^3 - (h_{k-1} - z)^3)/(1 - v_k{}^2/E_k) \tag{9}$$

$$\mu_{eff} = (1/D)\sum_{k=1}^{2}\rho_k t_k \tag{10}$$

ρ_k represents the density, while h_k represents the height of each layer. When solving (13) for the $1/k_m$ mechanical compliance, one obtains:

$$1/k_m = r^2/2\pi D I_e \tag{11}$$

Solving gives the following equation for the electromechanical coupling ratio:

$$\eta = 2\pi I_m e_{31,f} z \tag{12}$$

The circular plate formula [35] is used to determine the natural frequency:

$$f_n = (\lambda_{01}/r)^2 \sqrt{D/\mu_{eff}} \tag{13}$$

where λ_{01} is the vibration mode (01) eigenvalue. The mass of the composite disk as a whole, m_d. In addition, the shape function is utilized to calculate the modal mass:

$$m_d = (\rho_{\rho\rho} t_{\rho\rho} + \rho_{be} t_{be}) \pi r^2 \tag{14}$$

$$m_m = m_d * 2 \int_0^1 \varphi(x_\vartheta)^2 x_\vartheta dx_\vartheta \tag{15}$$

where the densities of the layers are $\rho_{\rho\rho}$ and ρ_{be} respectively. The Finite element modeling of the device was made using COMSOL®. Von Mises stress analysis is given in Figure (2). A linear effect can be observed under different pressure loads on the circular plates. To present the maximum load on the plate surface, a static structural simulation was done and the load is adjusted from the values taken from the experiment setup.

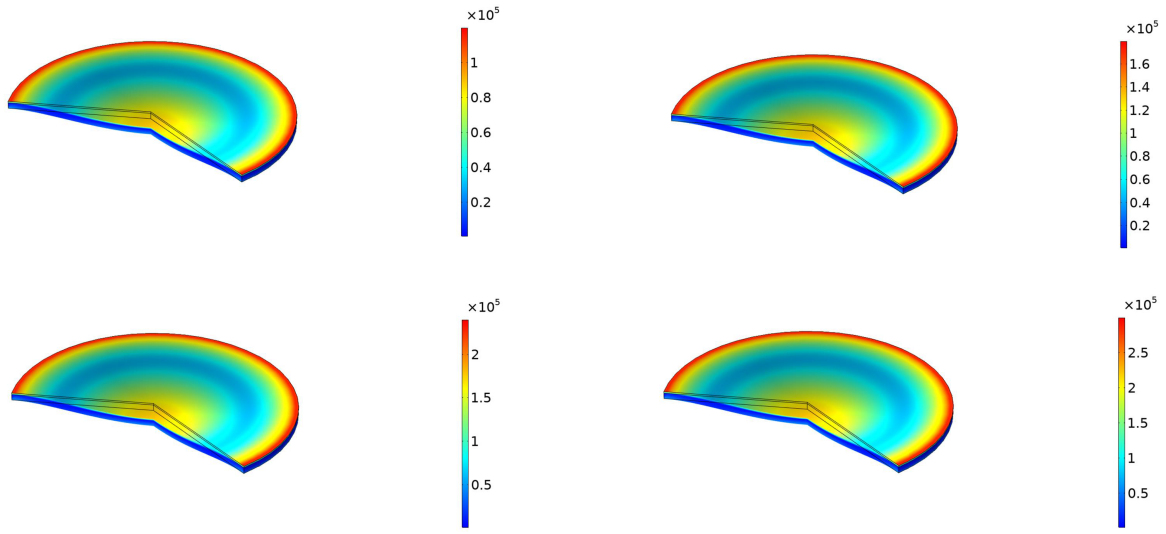

Figure 2. Von Mises stress analysis of circular plates for different wind pressure inputs: a) 200 Pa b) 300 Pa c) 400 Pa d) 500 Pa pressure.

To visualize the modal frequencies of the circular plate, a FEM model for modal analysis is given in Figure (3). The geometry was defined as a circular plate with the radius of the harvester plates. Built-in PVDF-TrFE and PVC materials were used for piezoelectric and structural layers, respectively. The plate was fixed from the boundaries and run under simulation with fine mesh. Using (13), a 10.3% error was found between the analytical and the FEM model in the first resonance frequency for validation.

The simulation was run for increasing radius values for 400 Pa pressure input. For different parametric measurements, mechanical properties and voltage output of the device for optimization are given in Figure (4).

The frequency response of the circular plate is given in Figure (5). Phase change, amplitude, damping ratio, and quality factor values are given.

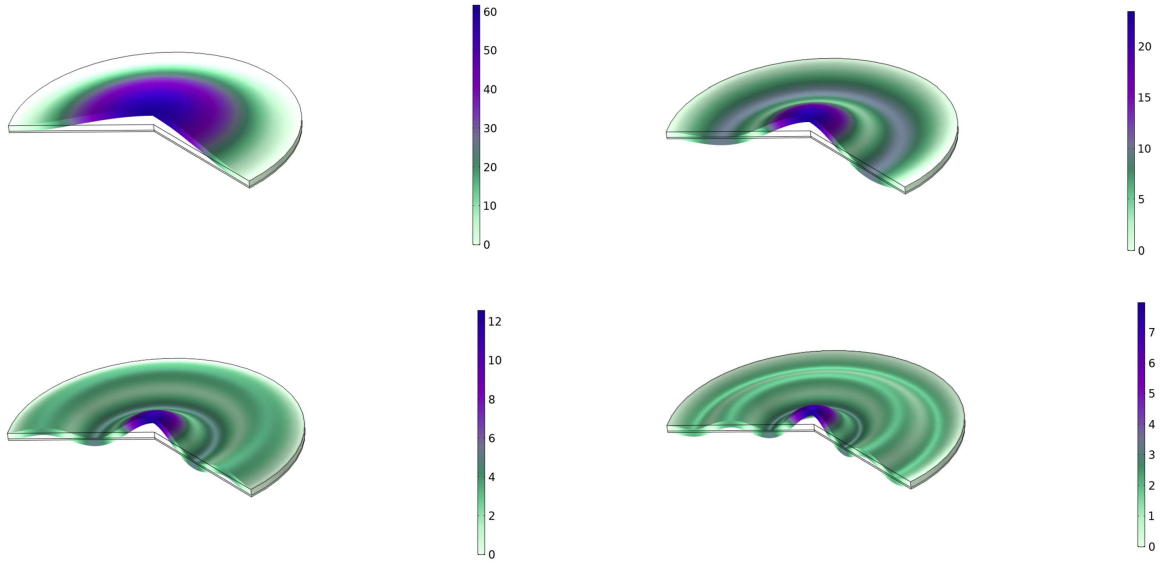

Figure 3. Modal analysis of circular plates for 4 respective resonance frequencies: a) First resonance frequency: 9.74 kHz, b) Second resonance frequency: 36.44 kHz, c) Third resonance frequency: 77.30 kHz, d) Fourth resonance frequency: 128.91 kHz.

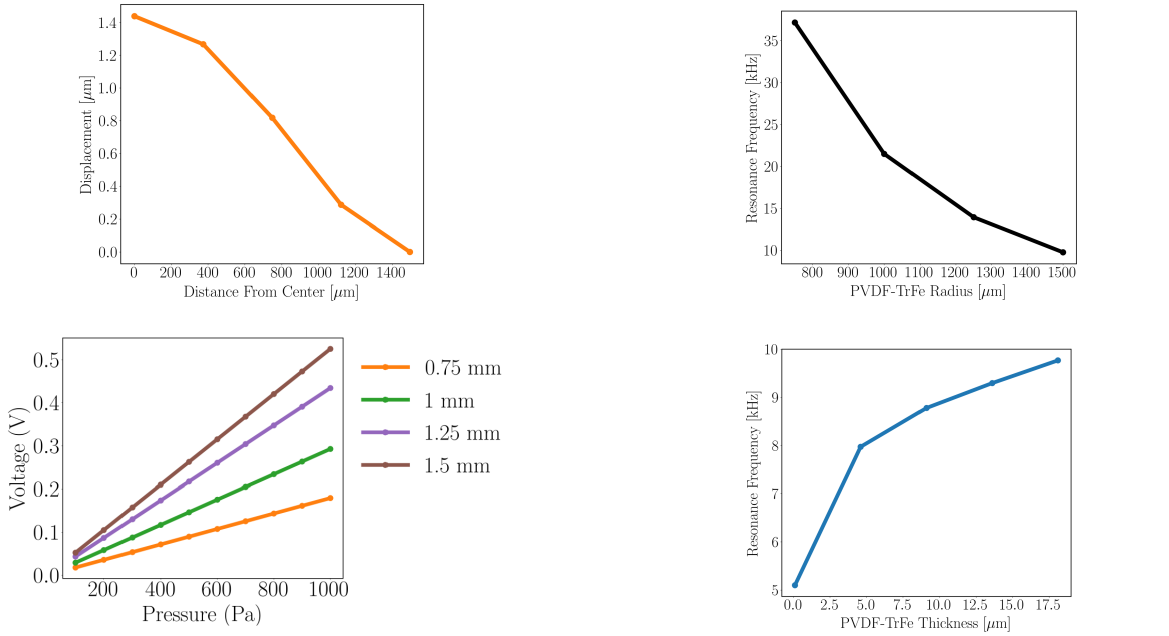

Figure 4. Mechanical properties of the device for optimization: a) Displacement of a selected point on the plate surface for increasing distance from the center b) Resonance frequencies for increasing radius c) Voltage outputs of the circular plates for increasing pressure values d) Resonance frequencies for increasing thickness.

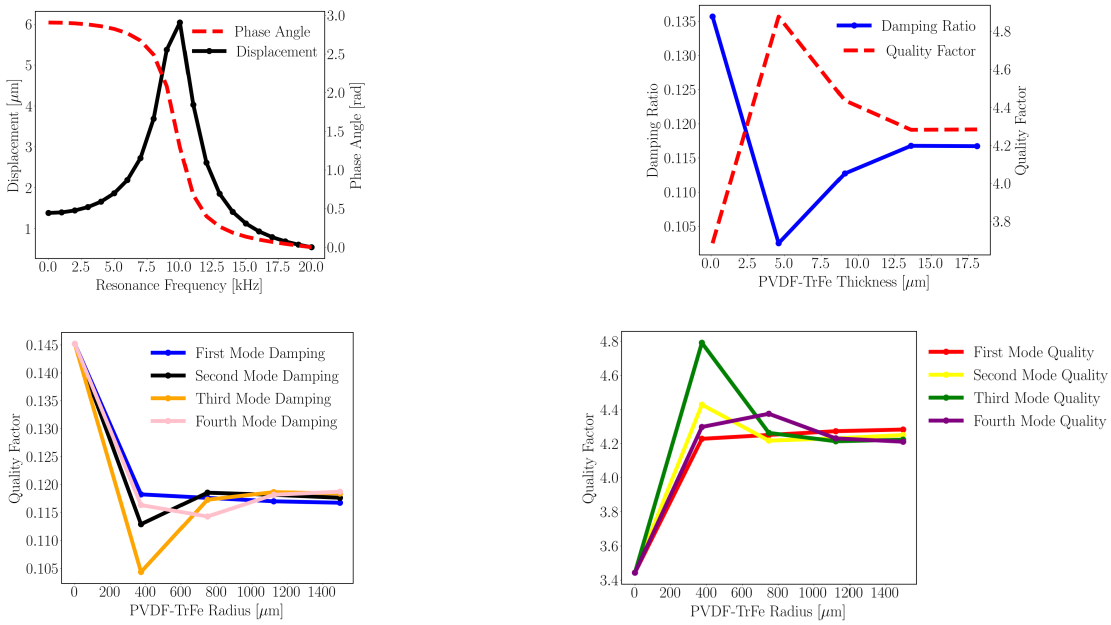

Figure 5. Frequency response plots of the circular plate: a) Frequency response of the plate for phase change and amplitude b) Damping ratio and quality factor of the plate change for increasing piezoelectric layer thickness c) Damping factor changes for increasing plate radius d) Quality factor changes for increasing plate radius.

3. Results and discussion

An 18 µm PVDF-TrFE layer was then placed on the double-sided tape. Two 3×3 mm electrode pads were cut out of the PVDF-TrFE film to make bonding easier while getting connections from the device. The sheet was metal coated on both sides. A circular plate energy harvester with 3 mm diameter circular plates was fabricated. A finite element model was developed to measure the resonance frequency of the device. An axisymmetric geometry was run under FEM simulation.

The experimental platform was constructed as depicted in Figure (6) with the device under test. The configuration included a 4-wire Pulse Width Modulation (PWM) fan, an Arduino Uno, a dry air source, and an Adafruit BMP280 pressure sensor breakout board. The wind pressure affected on the energy harvester was calculated as 400 Pa.

A code was built to sense pressure from serial pins dynamically. The Serial Peripheral Interface (SPI) protocol was utilized for communication. Using 3D-printed components, a novel test setup was built. Dry air was directed toward the fan's rotating propeller, which generates pressure fluctuations by generating intervals. The frequency of these intervals was determined by adjusting the fan's PWM frequency and operating voltage. PEH was attached close to the fan, so these variations could vibrate it to generate alternating voltage. The maximum wind speed recorded was 72 km/h. The fan's rotational speed was confirmed using a tachometer.

Figure (7) depicts the energy harvester's voltage output under wind load without any external circuit connection and the test setup. A 10.1% error between the experimental maximum voltage value of 756 mV and the FEM result was calculated for wind pressure application of 400 ± 30 Pa. During the wind tests, in 10-s intervals, a 3-s wind flow was followed with a 4-s break and a 3-s flow again. Voltage production can be observed in the first and the last interval.

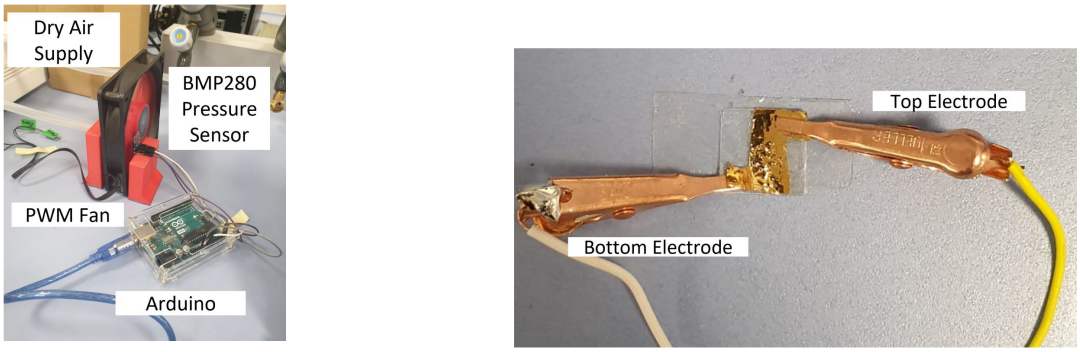

Figure 6. The piezoelectric harvester is shown under test: a) 3D-printed parts with a cavity for dry air supply and a surface for mounting the BMP280 pressure sensor were used to construct the test setup to characterize the wind flow affecting the energy harvester. SPI communication was utilized to obtain the results from the BMP280 pressure sensor b) The piezoelectric energy harvester was run under wind test getting connections from both electrodes with a similar test setup as BMP280. Instead of the Arduino connection, the electrodes of the energy harvester were connected to an oscilloscope to measure voltage output under the wind.

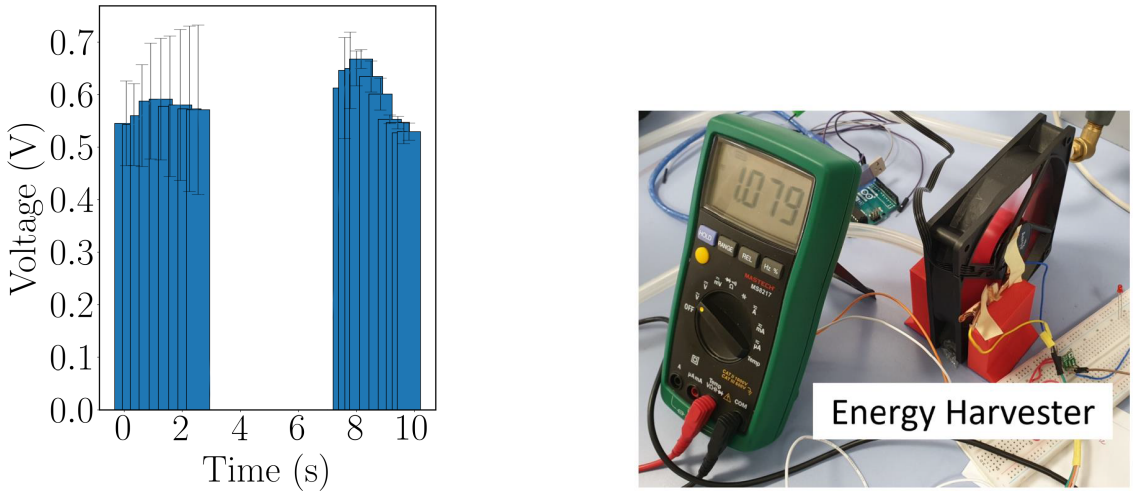

Figure 7. Frequency response plots of the circular plate: a) V_{max} was measured as 984 mV from the wind tests, error bars are plotted from 3 consecutive trials b) The energy harvester was run under wind tests, voltage output was first validated with a multimeter.

4. Conclusion

In this study, the mechanical and electrical characteristics of a piezoelectric wind energy harvester are given. The properties of the output voltage were examined using a wind test instrument. For von Mises stress and modal analysis, finite element modeling (FEM) was used. The circular plate's resonance frequency sweeps, quality factors, and damping ratios were given numerically. For a PVDF-TrFe piezoelectric layer with a thickness of 18 µm and a radius of 1.5 mm, the damping ratio and quality factor were calculated to be 0.117 and 4.284, respectively. V_{max} was determined to be 984 mV based on the wind configuration and compared to the FEM outputs. For further improving the harvester design, a low-voltage dropout rectifier circuit can be built to show the capacitor/battery charging capacity. Extensive material characterization studies can be conducted to make a better comparison between microfabricated energy harvesters with actuator layers built using PVDF-TrFE.

References

[1] Qian F, Hajj MR, Zuo L. Bio-inspired bi-stable piezoelectric harvester for broadband vibration energy harvesting. Energy Conversion and Management 2020; 222: 113174. doi:10.1016/j.enconman.2020.113174

[2] Li X, Yu K, Upadrashta D, Yang Y. Multi-branch sandwich piezoelectric energy harvester: mathematical modeling and validation. Smart Materials and Structures 2019; 28 (3): 035010. doi:10.1088/1361-665x/aaf8bf

[3] Ramírez JM, Gatti CD, Machado SP, Febbo M. A piezoelectric energy harvester for rotating environment using a linked E-shape multi-beam. Extreme Mechanics Letters. 2018; doi:10.1016/j.eml.2018.12.005

[4] Toprak A, Tigli O. Piezoelectric energy harvesting: State-of-the-art and challenges. Applied Physics Reviews 2014; 1 (3): 031104. doi:10.1063/1.4896166.

[5] Morimoto K, Kanno I, Wasa K, Kotera H. High-efficiency piezoelectric energy harvesters of c-axis-oriented epitaxial PZT films transferred onto stainless steel cantilevers. Sensors and Actuators A: Physical 2010; 163 (1): 428–432. doi:10.1016/j.sna.2010.06.028.

[6] Horowitz SB, Sheplak M, Cattafesta LN, Nishida T. A MEMS acoustic energy harvester. Journal of Micromechanics and Microengineering 2006; 16 (9): S174–S181. doi:10.1088/0960-1317/16/9/s02

[7] Wang X, Song J, Liu J, Wang ZL. Direct-Current Nanogenerator Driven by Ultrasonic Waves. Science 2007; 316 (5821): 102–105. doi:10.1126/science.1139366

[8] Hu Y, Zhang Y, Xu C, Lin L, Snyder RL et al. Self-Powered System with Wireless Data Transmission. Nano Letters 2011; 11 (6): 2572–2577. doi:10.1021/nl201505c

[9] Hu Y, Xu C, Zhang Y, Lin L, Snyder RL et al. A Nanogenerator for Energy Harvesting from a Rotating Tire and its Application as a Self-Powered Pressure/Speed Sensor. Advanced Materials 2011; 23 (35): 4068–4071. doi:10.1002/adma.201102067

[10] Lin L, Hu Y, Xu C, Zhang Y, Zhang R. et al. Transparent flexible nanogenerator as self-powered sensor for transportation monitoring. Nano Energy 2013; 2 (1): 75–81. doi:10.1016/j.nanoen.2012.07.019.

[11] Ueberschlag P. PVDF piezoelectric polymer. Sensor Review 2001; Vol. 21 No. 2, pp. 118-126. doi:10.1108/02602280110388315

[12] Mohammadi B, Yousefi AA, Bellah SM. Effect of tensile strain rate and elongation on crystalline structure and piezoelectric properties of PVDF thin films. Polymer Testing 2007; 26 (1): 42–50. doi:10.1016/j.polymertesting.2006.08.003

[13] Davis GT. Production of Ferroelectric Polymer Films. In: Wang T.T., Herbert J.M., Glass A.M. (Eds.), The Applications of Ferroelectric Polymers Blackie and Sons Ltd, Glasgow, USA, 1988.

[14] Kepler RG, Anderson RA. Ferroelectricity in polyvinylidene fluoride, Journal Applied Physics 49 1978; 1232.

[15] Lovinger AJ. Poly(vinylidene fluoride). In: Bassett D.C. (Ed.), Developments in Crystalline Polymers, Applied Science Publishers, London, 1982.

[16] Hayakawa R, Wada Y. Piezoelectricity and related properties of polymer films, Adv. Polym. Sci. 11 1973; 1.

[17] Broadhurst MG, Davis GT, McKinney JE, Collins RE. Piezoelectricity and pyroelectricity in Poly(vinylidene fluoride)— a model, Journal Applied Physics 1978; 49 (10):4992.

[18] Purvis CK, Taylor PL. Piezoelectricity and pyroelectricity in poly(vinylidene fluoride): influence of the lattice structure, Journal Applied Physics 1983; 54: 1021.

[19] Salimi A, Yousefi AA. FTIR studies of β-phase crystal formation in stretched PVDF films. Polym. Testing 2003; 22 699.

[20] Schwartz M. Encyclopedia of Smart Materials, vols. 1–2, Wiley, New York 2002; 811.

[21] Katsouras I, Asadi K, Li M, van Driel TB, Kjær KS et al. The negative piezoelectric effect of the ferroelectric polymer poly(vinylidene fluoride) Nature Materials 2015;15 (1): 78–84. doi:10.1038/nmat4423.

[22] Lindner M, Hoislbauer H, Schwodiauer R, Bauer-Gogonea S, Bauer S. Charged cellular polymers with "ferroelectretic" behavior. IEEE Transactions on Dielectrics and Electrical Insulation 2004; 11 (2): 255–263. doi:10.1109/tdei.2004.1285895

[23] Bystrov VS, Paramonova EV, Bdikin IK, Bystrova AV, Pullar RC et al. Molecular modeling of the piezoelectric effect in the ferroelectric polymer poly(vinylidene fluoride) (PVDF). Journal of Molecular Modeling 2013; 19 (9): 3591–3602. doi:10.1007/s00894-013-1891-z

[24] Demartino C, Quaranta G, Maruccio C, Pakrashi V. Feasibility of energy harvesting from vertical pedestrian-induced vibrations of footbridges for smart monitoring applications. Comput Aided Civ Inf. 2022; 37: 1044– 1065. https://doi.org/10.1111/mice.12777.

[25] Kunkel HA, Locke S, Pikeroen B. IEEE Trans. Ultrason. Ferroelect. Freq. Control 37 1990; 316.

[26] Tian W, Ling Z, Yu W, Shi J. A Review of MEMS Scale Piezoelectric Energy Harvester. Applied Sciences 2018; 8(4): 645. doi:10.3390/app8040645

[27] Machado R, Santos VBD, Ochoa DA, Cerdeiras E, Mestres L et al. Elastic, dielectric and electromechanical properties of (Bi0.5Na0.5)TiO3-BaTiO3 piezoceramics at the morphotropic phase boundary region. J. Alloys Compd. 2017; 690, 568–574.

[28] Sappati K, Bhadra S. Piezoelectric Polymer and Paper Substrates: A Review. Sensors 2018; 18 (11): 3605. doi:10.3390/s18113605

[29] Ueyama T, Yamana S, Kaneko N. Sintering Properties of BaTiO3 Green Sheets with High Packing Density. Japanese Journal of Applied Physics 1987; 26 (S2): 139. doi:10.7567/jjaps.26s2.139

[30] Piezotech, Piezoelectric films technical information.

[31] Evans J. Piezoelectric-Based, Self-Sustaining Artificial Cochlea, 2014.

[32] Xikang Y, Jiapeng W. Study on factors influencing the performance of reactive powder concrete. IOP Conference Series: Earth and Environmental Science 2020; 510. 052075. 10.1088/1755-1315/510/5/052075

[33] Do B, Valerii C, Le D, Evgenia K, Pham T et al. Applied theory of bending vibration of the piezoelectric and piezomagnetic bimorph. Journal of Advanced Dielectrics 2020; 10. doi:10.1142/S2010135X20500071

[34] Shelton SE. Piezoelectric Micromachined Ultrasound Transducers for Air-coupled Applications. University of California Davis, 2014.

[35] Reddy JN. Theory and Analysis of Elastic Plates and Shells. Taylor and Francis, 2007.

[36] Muralt P, Ledermann N, Paborowski J, Barzegar A, Gentil S et al. Piezoelectric micromachined ultrasonic transducers based on PZT thin films, IEEE Trans. Ultrason., Ferroelectr. 2005; Freq. Control, vol. 52, pp. 2276-2288

[37] Lu Y. Piezoelectric Micromachined Ultrasonic Transducers for Fingerprint Sensing. University of California Davis, 2015.